Probabilistic Engineering Mechanics 78 (2024) 103689

Contents lists available at ScienceDirect

Probabilistic Engineering Mechanics

journal homepage: www.elsevier.com/locate/probengmech

Real-time anomaly detection of the stochastically excited systems on spherical (S^2) manifold

Satyam Panda [a,*], Breiffni Fitzgerald [a], Budhaditya Hazra [b]

[a] Department of Civil, Structural and Environmental Engineering, Trinity College Dublin, Dublin D02 PN40, Ireland
[b] Department of Civil Engineering, Indian Institute of Technology, Guwahati, Assam, India

ARTICLE INFO

Keywords:
Condition monitoring
Manifolds
Stochastic dynamics
Lie algebra
PGA
Differential geometry

ABSTRACT

Advanced analytical tools have become crucial in today's constantly changing and complex systems. Real-time Principal Geodesic Analysis (RPGA) is a novel technique that provides a unique perspective for analyzing nonlinear data on differentiable manifolds. Traditional linear methods are often inadequate when exploring the complexities of such data. Orthogonal transformation techniques such as Principal Component Analysis (PCA) and Principal Geodesic Analysis (PGA) are highly desirable for condition monitoring stochastically excited systems in domains like mechanical, aerospace, and civil engineering. However, uncertainties and dynamic fluctuations necessitate robust analytical methods for early change detection to ensure safety, performance, and cost-effectiveness. Limitations posed by linear orthogonal transformation techniques such as PCA and its recursive counterparts make it imperative to adapt these techniques to nonlinear situations where data does not evolve in a flat Euclidean space. Significant advancements have been made in this field over recent decades, with data-driven real-time algorithms such as RPCA, RCCA, and RSSA providing reliable solutions for complex multidimensional problems. However, for curved space, the nonlinear RPGA technique takes center stage. It is known for its effectiveness in extracting meaningful information from the complex data stream. This paper explores the foundational concepts and methodologies underlying the transition from linear to nonlinear data analysis. By examining examples such as stochastic geometric oscillator on S^2, and the inverted spherical pendulum cart system navigating a rough surface, we illustrate the significance of reliable, real-time damage detection techniques provided by tools such as RPGA.

1. Introduction

In the field of complex dynamical systems, which often involve interactions between geometry and stochasticity, there is a growing need for advanced analytical tools that can help unravel the complexities of these systems [1–4]. One of the biggest challenges in this field is exploring geometric nonlinear data, where traditional linear methods fail to provide accurate insights. To effectively perform this analysis, Principal Component Analysis (PCA) and its recursive counterpart, RPCA, prove to be useful starting tools [5–10]. Over the past decades, remarkable progress has been made in the field of condition monitoring on Euclidean spaces, with the development of algorithms for damage detection, modal identification, and control [8,10,11]. Traditional algorithms, though effective, are often limited by their offline nature and are unsuitable for time-varying systems, such as condition monitoring of wind turbines [12,13], bridge–vehicle interactions [14], and tuned mass dampers, which are prone to frequent detuning due to changing load conditions [15,16], ambient variations, and damages [17]. In response to these challenges, a new generation of data-driven, real-time algorithms have emerged, including real-time Principal component analysis (RPCA), recursive canonical correlation analysis (RCCA), and recursive singular spectrum analysis (RSSA), providing more reliable solutions for complex multidimensional problems [9,10]. However, these techniques are inherently linear, rooted in linear algebra, and thus require data to reside within Euclidean space. Given the constraints imposed by these linear techniques, it becomes imperative to adapt and redesign them for nonlinear situations where data resides on a differential manifold [18,19]. Recent advances, such as those utilizing Isogeometric Analysis based on extended Catmull–Clark subdivision, have shown promise in maintaining geometric exactness while allowing for refined analysis [20]. Additionally, methods like quasi-harmonic Bézier approximation offer innovative approaches to construct minimal surfaces from given boundaries, demonstrating the efficiency and applicability of such techniques in complex modeling scenarios [21].

The aim for addressing the aforementioned constraints leads to data-driven methodologies like Principal Geodesic Analysis (PGA), rapidly

* Corresponding author.
E-mail address: pandasa@tcd.ie (S. Panda).

https://doi.org/10.1016/j.probengmech.2024.103689
Received 14 July 2024; Received in revised form 26 August 2024; Accepted 19 September 2024
Available online 28 September 2024

gaining ground as a prominent approach to understand the dynamics of nonlinear systems [3,4]. PGA considers the scale and curvature effects within the analysis, enabling a comprehensive understanding of the underlying geometric structures [22]. Similar to PCA [6,8], PGA operates on response data, albeit focusing on nonlinear manifold structures inherent in the system's behavior. By capturing the intrinsic geometry of the data manifold, PGA facilitates the extraction of meaningful low-dimensional representations that encapsulate the system's underlying dynamics. This enables the monitoring of intricate systems with reduced computational overhead [3], a crucial advantage in real-time condition monitoring (CM) applications. The essence of PGA lies in its ability to uncover the intrinsic geometric structure of the system's response data, thereby serving as a sensitive indicator of its current state. However, the limitation of PGA lies in its inability to adapt to real-time applications. The transition from PGA to Real-time Principal Geodesic Analysis (RPGA) represents a natural evolution in CM methodologies, addressing the need for adaptive and real-time techniques to accommodate real-time structural conditions.

By iteratively updating the geodesic structure of the data manifold, RPGA provides a mechanism for continuous monitoring and adaptation, crucial for ensuring the reliability and accuracy of anomaly detection in evolving systems. One compelling real-world motivation for RPGA is the domain of condition monitoring (CM) for stochastically excited systems that span applications as diverse as aerospace, civil engineering, and mechanical systems. In such systems, the inherent uncertainties and dynamic fluctuations necessitate robust analytical methods for the early detection of damage, which can have implications for safety, performance, and cost-effectiveness. By examining real-world examples such as the condition monitoring of wind turbines [3], computer vision application [23], and the behavior of Pendulum tuned mass dampers (TMDs) [24], the critical need for a tool like RPGA can be witnessed. These systems are highly susceptible to changing environmental conditions, loading variations, and structural damage, underscoring the significance of reliable, real-time damage detection techniques.

The primary objective of this work is to develop and demonstrate the efficacy of RPGA in real-time condition monitoring of complex systems residing on curved spaces. By leveraging RPGA's capability to capture the intrinsic geometric structure of nonlinear data manifolds adaptively, our aim is to provide a robust framework for early detection of structural damage and dynamic changes in evolving systems. Numerous numerical examples validate RPGA's performance for the systems with stochastic excitations. By monitoring key indicators derived from the system's response data, such as vibration patterns and dynamical changes, RPGA aims to facilitate timely intervention and maintenance scheduling, enhancing operational safety and cost-effectiveness in critical infrastructure. Through this investigation, we aspire to contribute to the advancement of condition monitoring methodologies, particularly in domains where traditional linear techniques prove inadequate in capturing the intricate dynamics of evolving systems.

The present study makes several novel contributions to the field of condition monitoring for manifold-based applications, outlined as follows: Firstly, the study introduces Real-time Principal Geodesic Analysis (RPGA) as a novel framework specifically designed for analyzing data residing on differential manifolds. This is a significant departure from traditional techniques like PCA and RPCA, which are tailored for Euclidean spaces. RPGA transcends the limitations posed by linear techniques by leveraging the inherent geometric complexities of systems with nonlinear behaviors and complex geometries. The proposed RPGA framework significantly differs from the work in literature [25], even both methods share the same name, the underlying theories and implementation strategies are distinct. Literature [25] focuses on recursively removing variability in the principal geodesic directions within homogeneous spaces whereas proposed RPGA in this work is based on Eigen perturbation theory which ensures stability and adaptability in capturing the data's evolving structure making it more effective for analyzing dynamic systems. This aspect expands the scope of condition monitoring methodologies to effectively analyze diverse and intricate systems. Secondly, RPGA enables continuous monitoring and adaptation by iteratively updating the geodesic structure of the data manifold. This feature is crucial for accurate anomaly detection in evolving systems, which is not adequately addressed by existing methods. Finally, the efficacy of RPGA is demonstrated through numerical investigations on various systems such as stochastic geometric oscillator on $\mathbb{S}^2$, and the inverted spherical pendulum cart system. These investigations validate RPGA's effectiveness in detecting damage, thereby reinforcing its significance in advancing condition monitoring methodologies.

2. Background

In the field of manifold analysis, various mathematical concepts are essential. Consider a group $\mathcal{M}$, which represents a curved space known as a Riemannian manifold. At any point x on this manifold, there exists a tangent space, denoted as $T_x\mathcal{M}$, which essentially describes the directions in which one can move from x. The collection of all these tangent spaces across the manifold forms what is known as the tangent bundle, represented as $\mathcal{T}\mathcal{M}$. A key element within this manifold is the local metric, which helps measure lengths and angles. This metric provides a way to calculate the norm (or size) of any vector V in the tangent space at x, denoted as $\|V_x\|$. Additionally, for a function ψ that maps real numbers to points on the manifold, the Riemannian gradient at any point x on the manifold is a vector indicating the direction of steepest ascent of ψ.

Now, let us delve into the notion of the covariant derivative. For a vector field $w \in \mathcal{T}\mathcal{M}$, the covariant derivative in the direction of $v \in T_x\mathcal{M}$ is represented as $\nabla_v w$. We assume that $\mathcal{M}$ possesses a metric connection, as described in [19]. To facilitate the movement of tangent vectors between different points on the manifold, the parallel transport operator, denoted as $P_r^{(x\to y)}$. It efficiently transports a tangent vector from $T_x\mathcal{M}$ to $T_y\mathcal{M}$. For a more simplified viewpoint of expressing manifold as a locally Euclidean, the manifold exponential map is employed, defined as $\exp : \mathcal{T}\mathcal{M} \to \mathcal{M}$, with the action $exp_x(v)$. Its inverse operation, referred as 'log', is locally defined and denoted as $log_y x$, where $y \in \mathcal{M}$. To quantify the separation between two points within the manifold $\mathcal{M}$, we introduce the Riemannian distance, denoted as $d(x, y)$. With this notation in place, now these mathematical entities can be individually defined as:

1. Metric tensor: Like the inner product $(\cdot)$ in Euclidean space, a metric tensor, represented as $\mathbf{g}$, is a fundamental building block in differential geometry for a manifold $\mathcal{M}$. It makes defining distances and angles easier. Metric tensors defined at each point $p \in \mathcal{M}$ that smoothly fluctuate with p make up the metric tensor $\mathbf{g}$ on $\mathcal{M}$. A metric tensor is a bilinear form defined on the tangent space at every given point $p \in \mathcal{M}$. The metric tensor can be defined in two different ways. These are
   (a) *Intrinsic Approach*: The intrinsic approach in differential geometry is a foundational framework for characterizing geometric structures without reference to external coordinates or embeddings. It revolves around the notion of an intrinsic metric tensor, denoted as $\mathbf{g}$, which defines the inner product between tangent vectors at each point on the manifold. Geodesics, described by the equation $\nabla_{\dot{\gamma}}\dot{\gamma}$, are the paths of shortest distance on the manifold, and they provide essential information about the geometry. In this approach, the focus is on the intrinsic properties of the manifold, where the covariant derivative $\nabla_{(\cdot)}(\cdot)$ encodes information about how vectors change as they move along the manifold. This approach enables the characterization of curvature and other geometric properties directly on the manifold, independent of any external reference.

(b) *Extrinsic Approach*: The extrinsic view of a manifold involves embedding it within a higher-dimensional space. Mathematically, a manifold can be described by an equation that delineates the points it occupies within the ambient space. For example, when viewed extrinsically, the unit sphere is perceived as a subset of three-dimensional Euclidean space. This perspective is often referred to as the "bird's eye view." In this context, the manifold can be expressed as: $\mathcal{M} \subset \mathbb{R}^n$, where $\mathcal{M}$ represents the manifold of interest, and $\mathbb{R}^n$ denotes the higher-dimensional ambient space in which it is embedded. This extrinsic view provides a means of understanding the manifold's relationship with its containing space.

2. Geodesics: The straightest possible path, referred to as a geodesic, between two points on a surface can be mathematically defined. A geodesic is essentially a curve that locally minimizes its length, and it represents the path that a non-accelerating particle would follow. In the context of flat planes, geodesics are akin to straight lines. However, on a spherical surface, geodesics manifest as large circles. These geodesics are intrinsically linked to the Riemannian metric, which also influences the concepts of distance and acceleration within a space, as documented in [26]. Geodesics possess several intriguing properties, including preserving a consistent direction on a given surface. Furthermore, any point along a geodesic arc can be associated with a normal vector that remains parallel to the surface at that specific location. The Equation of Geodesic is given by:

$$\frac{d^2u^k}{d\lambda^2} + \Gamma^k_{ij}\frac{du^i}{d\lambda}\cdot\frac{du^j}{d\lambda} = 0 \tag{1}$$

3. Parallel Transport: Parallel transport is a fundamental technique in geometry employed to transport geometric information along geodesic paths within a manifold. When a manifold is equipped with an affine connection, it becomes possible to move vectors within the manifold along curves while ensuring their parallelism concerning the connection. Consequently, the parallel transport, associated with a specific connection, serves as a mechanism for seamlessly connecting the geometries of nearby points or locally altering the manifold's geometry along a given curve. It is worth noting that while there may exist various parallel transport concepts, this definition pertains to one specific method of linking the geometries of points along a curve [27]. The notion of covariant derivative is closely tied to the notion of parallel transport along a curve. The parallel transport operator, denoted as $\mathrm{P}_r^{x\to y}$, is a tool that helps move vectors along a curve γ on a manifold without changing their direction relative to the curve. Suppose we have a curve γ that starts at point x' and moves through the manifold. For vectors u and w at the starting point, the parallel transport keeps the inner product of these vectors constant along the curve. The covariant derivative, which measures how a vector field E changes as we move in a particular direction ω, is closely related to the parallel transport operator. If the vector field E does not change when parallel transported along the curve, then E is said to be parallel along that path. This condition is mathematically described by

$$\nabla_{\dot\gamma} E = 0 \tag{2}$$

A geodesic is a special type of curve on the manifold, where the direction of movement along the curve (represented by $\dot\gamma$) remains consistent as you move along the curve itself.

4. Exponential Mapping In the domain of Riemannian geometry, the exponential map plays a pivotal role. This mathematical map takes a subset of the tangent space T_pM of a Riemannian manifold M and maps it back onto the manifold itself. It is closely tied to the canonical affine connection established by the Riemannian metric. The behavior of geodesics, the paths of least distance on the manifold, is described by the geodesic equation, as expressed in [27]:

$$\ddot{x}^k + \sum_{i,j}\Gamma^k_{ij}(\gamma)\dot{x}^i\dot{x}^j = 0 \tag{3}$$

For any vector V in the tangent space T_xM at a point x on the manifold, there exists an interval I around the origin O and a unique geodesic $\gamma(t,x) : I \to M$ such that $\gamma(0) = x$ and $\dot\gamma = V$. This geodesic is precisely what the exponential map accomplishes, denoted as $\exp : T_xM \to M$. It maps each vector V in the tangent space to a point on the manifold, represented as $\exp_x(V)$. A manifold M is said to be geodesically complete if the domain of the exponential map, denoted as Exp, covers the entire tangent space T_xM for every x in M.

3. Notion of means on $\mathcal{M}$

To generalize means to manifolds, borrowing the knowledge from the Euclidean case is wise. The point $\bar{x}$, derived from a collection of points $x_1,\dots,x_N \in \mathbb{R}^d$, is defined as the average calculated as $\bar{x} = \frac{1}{N}\sum_{i=1}^N x_i$. This point possesses the special property of minimizing the sum of squared Euclidean distances to the given data.

$$\bar{x} = \underset{x\in\mathbb{R}^d}{\operatorname{argmin}} \sum_{i=1}^N \left\|x - x_i\right\|^2. \tag{4}$$

This well-established concept extends its reach by introducing a comprehensive range of mean estimators tailored to the specific distance metric under consideration. Given that the manifold might not conform to a linear space, the calculation of additive means may pose a challenge. One potential remedy for this challenge is employing the characterization mentioned above as an organic extension of the mean for nonlinear scenarios. Nevertheless, it is essential to acknowledge that this definition heavily relies on the chosen distance metric, which must be thoughtfully selected to achieve the most intuitively natural means of extension for manifolds. This consideration prompts us to explore a more suitable distance metric that inherently defines the mean, offering us an intrinsic definition of this fundamental statistical concept.

3.1. Extrinsic notion

In the context of an embedding represented by $\mathcal{R} : M^p \to \mathbb{R}^d$, the extrinsic mean is defined as:

$$\mu_\Phi = \underset{x\in M^p}{\operatorname{argmin}} \sum_{i=1}^N \left\|\Phi(x) - \Phi\left(x_i\right)\right\|^2 \;\forall x_1,\dots,x_N \in M^p \tag{5}$$

By utilizing the Euclidean norm, denoted as $|\cdot|$, on $\mathbb{R}^p$, the extrinsic mean can be equivalently computed as the conventional arithmetic mean of the transformed points $\Phi\left(x_i\right)$, followed by the projection of mean on M^p. To establish this equivalence, it is necessary to introduce a projection mapping $\pi : \mathbb{R}^d \to M^p$, which can be defined as follows:

$$\pi(x) = \underset{y\in M^p}{\operatorname{argmin}} \|\Phi(y) - x\|^2, \quad \forall x \in \mathbb{R}^p, \tag{6}$$

which leads to the following expression:

$$\mu_\Phi = \pi\left(\frac{1}{N}\sum_{i=1}^N \Phi\left(x_i\right)\right) \tag{7}$$

In Fig. 1, an example illustrating the extrinsic mean computation can be observed. This computation utilizes the gradient descent algorithm as defined in Eq. (5). In this illustrative example, we compute μ_Φ, for the data on the manifold embedded in $\mathbb{R}^3$. The process commences with an initial estimate of the mean, labeled as μ_0. The dotted lines on the graph show the objective function's equipotential levels. As the intensity drops, these lines change from red to blue, visually representing the optimization procedure. Iteratively, distance function minimizes, as

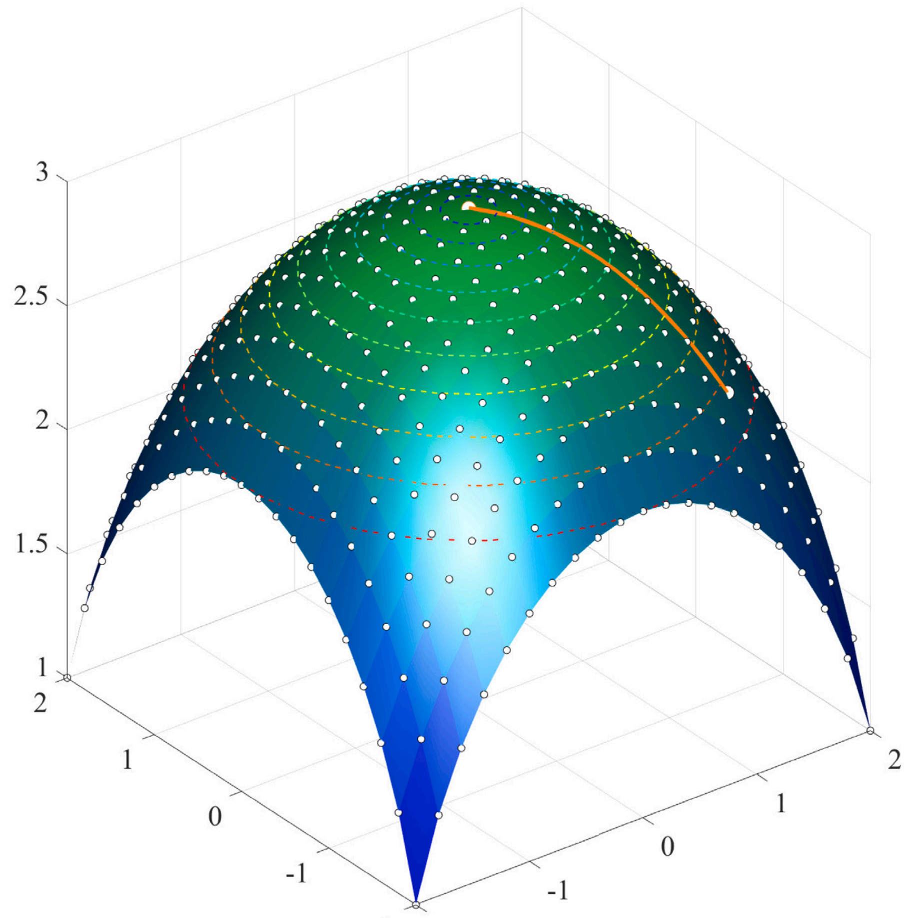

Fig. 1. Computing of the extrinsic mean. (For interpretation of the references to color in this figure legend, the reader is referred to the web version of this article.)

described in Eq. (5). This minimization entails successive steps, depicted by the orange trajectory in the graph. Nonetheless, this definition possesses certain limitations, primarily because it necessitates $\mathcal{M}$ to be embedded within $\mathbb{R}^n$. Expressing a manifold explicitly for every given problem may not always be feasible. Consequently, defining an extrinsic mean, contingent upon an additional embedding of the manifold, may not represent the most natural means of explaining the concept of a mean. This prompts us to consider a different strategy: creating a better distance metric to define the mean. Such an intrinsic definition of the mean would provide a more intuitive and flexible way to conceptualize this fundamental statistical concept.

3.2. Intrinsic notion

To derive a coherent definition of means on Riemannian manifolds, it is essential to leverage the inherent distance metric made available through a metric tensor on the manifold. This natural distance is known as the geodesic distance, and it exclusively relies on the intrinsic geometry of the manifold. Assuming a pathwise connected Riemannian manifold denoted as M^p and the natural geodesic distance function. Therefore, the intrinsic mean computation is analogous to the minimization of the sum-of-square distance function:

$$f(x) = \frac{1}{2N} \sum_{i=1}^{N} d\left(x, x_i\right)^2 \tag{8}$$

To guarantee that a solution to the optimization problem exists and is unique, we assume that the points $x_1, \dots, x_n \in M^p$ are situated within a compact and well-behaved region. To solve this problem, the study uses the widely known gradient descent algorithm, also referred to as the steepest descent method. In this context, the logarithmic map helps define the gradient of the function $f(x)$, guiding the optimization process. When the points $x_1, \dots, x_N$ are located within a neighborhood denoted as U, it becomes feasible to use the logarithmic mapping to express the geodesic distance, as indicated in Eq. (9). Consequently, for any pair of points x and y within this neighborhood, for all $x, y \in U$, the expression is as follows:

$$d(x, y) = \left\|\log_x(y)\right\| \tag{9}$$

Substituting Eq. (9) in Eq. (8), we get:

$$f(x) = \frac{1}{2N} \sum_{i=1}^{N} \left\|\log_x\left(x_i\right)\right\|^2 \; \forall\, x \in M^p \tag{10}$$

If we choose a point p that is near x, we can rewrite this function using a simplified notation, where $\tilde{x} = \log_p(x)$ and $\tilde{x}i = \log p\left(x_i\right)$. This results in:

$$f(x) \simeq= \frac{1}{2N} \sum_{i=1}^{N} \left\|\tilde{x} - \tilde{x}_i\right\|^2 \tag{11}$$

This expression is essentially the same as another function $\tilde{f}(\tilde{x})$. The point that minimizes this function, denoted by $\tilde{\mu}$, represents the average position of the points $\tilde{x}_i$ within a space that is similar to a flat Euclidean space $\mathbb{R}^p$:

$$\tilde{\mu} = \frac{1}{N} \sum_{i=1}^{N} \log_p\left(x_i\right) = \frac{1}{N} \sum_{i=1}^{N} \tilde{x}_i = \underset{\tilde{x} \in \mathbb{R}^p}{\operatorname{argmin}} \frac{1}{2N} \sum_{i=1}^{N} \left\|\tilde{x} - \tilde{x}_i\right\|^2 . \tag{12}$$

In this context, $\tilde{\mu}$ is a directional vector from point p to the function f's minimum. To compute $\nabla f(x)$, the process is reversed by parallel

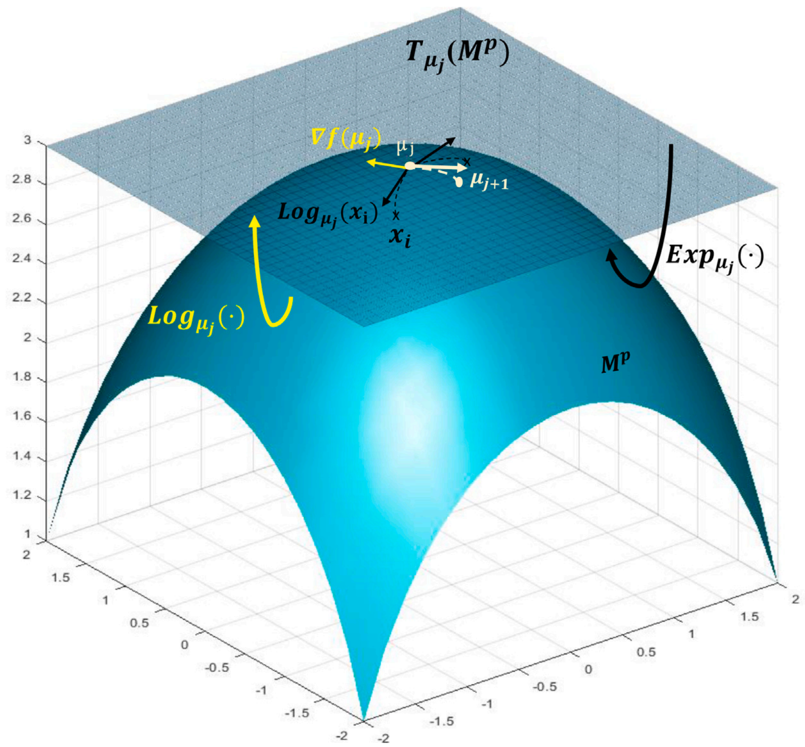

Fig. 2. An illustration of the intrinsic mean computation.

transporting $\tilde{\mu}$ along the minimal geodesic that connects points p and x.

$$\nabla f(x) = -\nabla_v \left(\frac{1}{N} \sum_{i=1}^{N} \log_p (x_i) \right) \tag{13}$$

The extrinsic mean, μ_j, is estimated as follows. The following equation describes updating this mean by making a single negative step. (also refer to Fig. 2):

$$\mu_{j+1} = \mathrm{Exp}_{\mu_j} \left(\frac{\tau}{N} \sum_{i=1}^{N} \log_{\mu_j} (x_i) \right) \tag{14}$$

In Eq. (14), the step size is represented by the parameter τ. Choosing the step size parameter τ and the initial estimate μ_0 of the intrinsic mean is important, as the gradient descent technique tends to converge locally. One of the data points, such as x_1, would be a good candidate for the initial estimate μ_0 given well-localized data. However, determining an appropriate value for τ is more nuanced and depends on the specific manifold. Fig. 2 illustrates a single step of the gradient descent algorithm to compute the intrinsic mean. With a current estimate denoted as μ_j, the algorithm calculates the gradient at this point and proceeds along the geodesic in the opposite direction for a duration of τ units of time.

4. Principal geodesics analysis

Let us introduce Principal Geodesic Analysis (PGA), which is similar to Principal Components Analysis (PCA) but designed specifically for curved spaces, or manifolds. Our goal is to work with a dataset represented as $x_1, \ldots, x_N \in \mathcal{M}^p$ and identify unique sequences of geodesic submanifolds. First, we aim to find a series of nested geodesic submanifolds, denoted as $\mathcal{H}1 \subsetneq \mathcal{H}2 \subsetneq \cdots \subsetneq \mathcal{H}_p = \mathcal{M}^p$. These submanifolds, known as principal geodesic submanifolds, help us efficiently explore the variability in the data by examining how the data points project onto each of these submanifolds.

Next, we consider a sequence of one-dimensional geodesic submanifolds, labeled as $V_1, \ldots, V_p \subset \mathcal{M}^p$. These are called the principal geodesic components and serve as a way to break down the data into "independent" components, similar to how PCA works with principal components. Essentially, PGA offers a customized method for analyzing data on manifolds, providing insights into their underlying structure and variability.

Consider a set of closely located points $x_1, \ldots, x_N \in \mathcal{M}^p$. We can calculate the intrinsic mean of this data, denoted as μ. Now, let us focus on a region $U \subset T_\mu(\mathcal{M}^p)$ around this mean, which includes the origin (0). We perform a local transformation called the exponential map, denoted by $\mathrm{Exp}\,\mu : U \to \mathrm{Exp}\,\mu(U)$. This region is special because any geodesic submanifolds within it have well-defined projections, ensuring their existence and uniqueness.

When projected onto the first main geodesic submanifold, $\mathcal{H}_1$, in this case, the variance of the data should be maximized. Making use of the diffeomorphism that the exponential map provides and ensuring well-defined projection, one can express $\mathcal{H}_1$ as $\mathcal{H}_1 = \mathrm{Exp}\,\mu\,(\mathrm{span}\,\{v1\} \cap U)$. To find the optimal direction v_1 within this submanifold, we seek the direction that maximizes the following expression:

$$v_1 = \underset{\|v\|=1}{\mathrm{argmax}} \frac{1}{N} \sum_{i=1}^{N} \left\| \log_\mu \left(\pi_{\mathcal{H}} (x_i) \right) \right\|^2, \tag{15}$$

where $\pi_{\mathcal{H}}$ denotes the projection onto $\mathcal{H}_1$. Once we have determined the first principal geodesic submanifold $\mathcal{H}1$, we set $V1 = \mathcal{H}1 = \mathrm{Exp}\,\mu(\mathrm{span} v_1 \cap U)$. Next, with $\mathcal{H}1$ defined, we can determine the second principal geodesic submanifold, denoted as $\mathcal{H}2$. This is constructed as $\mathcal{H}2 = \mathrm{Exp}\,\mu(\mathrm{span} v_1, v_2 \cap U)$. Here, the direction v_2 is chosen to maximize the variance of the data when projected onto this two-dimensional geodesic submanifold $\mathcal{H} = \mathrm{Exp}\,\mu(\mathrm{span} v1, v_2 \cap U)$.

$$v_2 = \underset{\|v\|=1}{\mathrm{argmax}} \frac{1}{N} \sum_{i=1}^{N} \left\| \log_\mu \left(\pi_{\mathcal{H}} (x_i) \right) \right\|^2. \tag{16}$$

The second principal geodesic component, denoted as V_2, is characterized by: $V_2 = \mathrm{Exp}\,\mu\,(\mathrm{span}\,\{v2\} \cap U)$.

Algorithm 1 principal geodesic analysis algorithm

Input: Correlated data on manifold: $X \in \mathcal{M}$
Obtain intrinsic mean ▷ Refer Eq. (2)
Project data on $T_X\mathcal{M}$ ▷ Use matrix logarithm
Apply PCA on $T_X\mathcal{M}$
Obtain transformed response on $T_X\mathcal{M}$ ▷ Refer Eqs. (15) and (16)
Project back data from $T_X\mathcal{M}$ to $\mathcal{M}$ ▷ Use matrix exponential
Output: Decorrelated data: $Y \in \mathcal{M}$

4.1. Computing PGA

Efficiently computing PGA hinges on an observation: once the tangent vector $v_k \in T_\mu(\mathcal{M}^p)$ are obtained, one can fully determine the geodesics $\mathcal{H}_k$ and V_k. Therefore, our primary focus is computation of v_k. Consider the scenario where $v_1, \ldots, v_{k-1} \in T_\mu(\mathcal{M}^p)$ are already computed, and our aim is to calculate v_k. Here's how one can proceed:

$$v_k = \underset{\substack{\|v\|=1 \\ v \in \operatorname{span}\{v_1,\ldots,v_{k-1}\}^\perp}}{\operatorname{argmax}} \frac{1}{N}\sum_{i=1}^{N}\left\|\log_\mu\left(\pi_{\mathcal{H}}\left(x_i\right)\right)\right\|^2, \tag{17}$$

where, $\mathcal{H} = \exp_\mu\left(\operatorname{span}\left\{v_1,\ldots,v_{k-1},v\right\} \cap U\right)$. Notably, since $\left\{v_1,\ldots, v_{k-1},v\right\}$ forms an orthogonal basis, one can transform the equation as follows:

$$v_k \simeq \underset{v \in \operatorname{span}\{v_1,\ldots,v_{k-1}\}^\perp}{\operatorname{argmax}} \frac{1}{N}\sum_{i=1}^{N}\left\langle \log_\mu\left(x_i\right), v\right\rangle^2. \tag{18}$$

To maximize $\operatorname{Var}\left(\langle\log\mu(xi), v_k\rangle\right)$, find $v_k \in \operatorname{span}\left\{v_1,\ldots,v_{k-1}\right\}^\perp$. This interpretation is essentially consistent with traditional Principal Component Analysis (PCA) calculated on the data $\log\mu(xi)$, under the assumption that the first $k-1$ principal components are represented by $v_1,\ldots,v_{k-1}$. Consequently, one can show by induction that the principal components of PCA computed on the data $\log\mu(xi)$ would yield a fair approximation for the v_k values. $\frac{1}{N}\sum_{i=1}^{N}\langle\log\mu(xi), v\rangle^2$ corresponds to the classic sample variance of the data $\log\mu(xi)$ projected onto the one-dimensional linear subspace spanned by v, since $T_\mu(\mathcal{M}^p)$ is a linear space. Thus, we can reinterpret Eq. (18) as follows. Once these principal components are obtained, the data in the tangent space $T_\mu(\mathcal{M}^p)$ can be decorrelated along the direction of the principal components v_k, denoted as $y_i = v_k\left(\pi_{\mathcal{H}}\left(x_i\right)\right)$. The decorrelated data on the given manifold can then be retrieved by applying the exponential map $\exp_\mu(yi)$ in the direction of the orthogonal basis v_k.

4.2. PGA and orthogonal projections

Geodesics, the fundamental paths on Riemannian manifolds, serve as crucial constructs in various fields, including differential geometry, physics, and machine learning. Notably, in shape analysis and manifold learning, geodesic paths play a pivotal role in capturing intrinsic structures and relationships within data. Principal Geodesic Analysis (PGA), a robust framework for analyzing shape spaces, leverages geodesic paths to uncover the underlying structure of data sets, enabling efficient representation, comparison, and interpolation of shapes. Building upon this foundation, we delve into the interaction between geodesics and orthogonal modes, exploring how geodesics can be conceptualized as orthogonal projections onto shape spaces, thus providing a comprehensive understanding of their geometric properties and applications. This investigation enriches our theoretical understanding of geodesics and paves the way for practical implementations in various data-driven tasks, from shape modeling to dimensionality reduction. Principal Component Analysis (PCA) involves deriving the principal components by identifying the eigenvectors of the covariance matrix of the data, which denote the directions of maximum variance. Each principal component v_i is orthogonal to the others, forming a basis for the data space. Similarly, Principal Geodesic Analysis (PGA) operates within the tangent space of a manifold. At every point p on the manifold, the tangent space (T_pM) encompasses all potential tangent vectors at that location, offering a local linear approximation to the manifold. The orthogonal modes on the tangent space, denoted as ξ_i, capture the local deformation of the manifold. These modes are obtained by analyzing the principal geodesics, which are the paths of maximum deformation along the manifold. Mathematically, the modes ξ_i are orthogonal and form a basis for the tangent space T_pM. For a manifold based dynamical system with the responses on manifold as $\mathbf{X} = \left[x_1,\ldots,x_N\right]$, the mean μ can be obtained using the Karchar's mean [28] and the covariance matrix $R = \frac{1}{N-1}\left[\log_\mu(\mathbf{X})\right]\left[\log_\mu(\mathbf{X})\right]^T$ can be expressed as a standard Eigenvalue problem as,

$$\mathbf{RV} = \mathbf{V}\boldsymbol{\Lambda} \tag{19}$$

where, $\mathbf{V}$ and $\boldsymbol{\Lambda}$ are the eigenvectors and eigenvalues on the T_pM. These eigenvectors can be used to obtain the orthogonal responses on T_pM as $\mathbf{V}^T\left(\log_\mu(\mathbf{X})\right)$ and then it can be projected back to the manifold as $\operatorname{Exp}_\mu\left(\mathbf{V}^T\left(\log_\mu(\mathbf{X})\right)\right)$. In Principal Component Analysis (PCA), each principal component captures a unique source of variation in the data. Similarly, in Principal Geodesic Analysis (PGA), each orthogonal mode signifies a distinct direction within the data space, representing specific patterns or structures inherent in the dataset. This framework finds applications in analyzing and understanding complex data on curved manifolds, such as shape analysis, image processing, and dimensionality reduction.

5. Proposed methodology

With a grasp of the underlying concept of the intrinsic mean, it becomes possible to define a real-time version of Principal Geodesics Analysis (PGA) as an analogue of Real-time Principal Components Analysis (RPCA) specifically designed for manifolds. The objective is to extract the principal geodesics, which play a crucial role in comprehending dynamical systems within the context of the present study. To begin this process, it is essential to comprehend the workings of Batch PGA, as it will furnish the initial estimates for the real time algorithm while ensuring its stability. Let us consider a set of points, denoted as $\mathbf{X} = \left[x_1,\ldots,x_N\right]$, belonging to the manifold M^p. The primary goal is to derive the principal geodesics, which are fundamental components for understanding the dynamics of the investigated systems. To achieve this, a real-time version of PGA is introduced, mirroring the Real-time Principal Components Analysis approach but tailored for manifolds. The initial step involves grasping the functioning of Batch PGA, which serves two purposes. Firstly, it provides the initial estimates required for the real-time algorithm to commence its iterative procedure. Secondly, it ensures the stability of the entire process. A preliminary understanding of the principal geodesics can be obtained by employing Batch PGA, serving as a solid foundation for the subsequent real-time analysis. A preliminary step in the Real-time Principal Geodesics Analysis (PGA) involves conducting Batch PGA using a batch of 100–500 samples from the dataset $\mathbf{X}$. The intrinsic mean of the batch data is calculated as follows:

$$\mu = \frac{1}{N}\sum_{i=1}^{N}\log_{x_1}\left(x_i\right) \tag{20}$$

In Eq. (20), x_i represents the ith sample in the dataset $\mathbf{X}$, and N denotes the total number of samples in the batch. The intrinsic mean, μ, estimates the batch data's central tendency in terms of their logarithmic coordinates concerning a chosen reference point, x_1. Subsequently, the batch data is projected onto the tangent space at the intrinsic mean, denoted as $T_\mu M^p$. This projection is necessary because the typical calculus operations are not directly defined on the manifold M^p. Transferring the batch data to the tangent space at the mean makes it feasible to perform computations and analyses analogous to $\mathbb{R}^p$, thus enabling the application of conventional mathematical techniques. The choice of the intrinsic mean as the reference point for the tangent space projection ensures that the resulting tangent space captures the local geometry of the data around the mean. This facilitates the processing and analysis of the data within the tangent space framework, enabling the application of statistical and geometric techniques well-defined in Euclidean spaces. By performing Batch PGA and projecting the data onto the tangent space at the intrinsic mean, the subsequent processing and analysis of the dataset $\mathbf{X}$ can be carried out effectively. This approach leverages the intrinsic mean as a reference point and utilizes the tangent space to perform computations and analyses analogous to those in Euclidean spaces. Therefore, the projected data can be written as $\log_{\mu}(x_i)$. This data is then utilized for the formation of data covariance matrix as,

$$\mathbf{R}_k = \frac{k}{k-1}\mathbf{R}_{k-1} + \frac{1}{k-1}\left[\log_{\mu}(x_k)\right]\left[\log_{\mu}(x_k)\right]^T \tag{21}$$

he subsequent crucial step in Principal Geodesics Analysis (PGA) involves the eigen decomposition of the covariance matrix. This process can be framed as an optimization problem known as the Standard Eigenvalue Problem (SEVP). Formally, the SEVP is defined as follows:

$$\max_{\mathbf{V}}\left(\mathbf{V}^T\mathbf{R}\mathbf{V}\right), \text{ subject to } \mathbf{V}^T\mathbf{V} = \mathbf{I}, \tag{22}$$

where $\mathbf{R} \in \mathbb{R}^{d\times d}$ is the covariance matrix. By solving this optimization problem, the matrices $\mathbf{V} \in \mathbb{R}^{d\times d}$ and $\boldsymbol{\Lambda} \in \mathbb{R}^{d\times d}$, which represent the eigenvalues and eigenvectors, respectively, are provided to the SEVP by the resultant solution. This can be expressed as in Eq. (19). The obtained solution from the SEVP represents the initial eigenspace, which serves as a basis for subsequent real-timeupdates in PGA. The real-timeupdate process consists of three main components: updating the intrinsic mean, updating the covariance matrix, and updating the eigenspace using an eigenperturbation technique. In each iteration of the real-timeupdate, the intrinsic mean is refined based on the updated estimates obtained from the previous iteration. This involves considering the logarithmic coordinates of the data points concerning the updated mean. Similarly, the covariance matrix is updated by incorporating the information from the updated intrinsic mean and the logarithmic coordinates of the data points. This updated covariance matrix captures the local variations and correlations within the dataset. Furthermore, the eigenspace is updated by applying an eigen perturbation technique, which involves incorporating minor variations to the eigenvectors and eigenvalues obtained from the previous iteration. This allows for adapting the eigenspace to capture the evolving data structure. By iteratively performing these three components, the real-time PGA algorithm refines the estimates of the principal geodesics, leading to an improved understanding of the dynamical systems under analysis. The real-timeupdate process ensures that the algorithm converges towards more accurately representing the underlying data structure, facilitating practical analysis and interpretation. Next, the expression for updating the mean is as follows, assuming a current estimate μ_k for the extrinsic mean:

$$\mu_{k+1} = \frac{1}{N}\mu_k + \mathrm{Exp}_{\mu_k}\left(\frac{N-1}{N}\sum_{i=1}^{N}\log_{\mu_k}(x_k)\right) \tag{23}$$

Consequently, it is possible to update the $\mathbf{R}$ iteratively as,

$$\mathbf{R}_k = \frac{k-1}{k}\boldsymbol{\Sigma}_k^{-1}\boldsymbol{\Sigma}_{k-1}\mathbf{R}_{k-1}\boldsymbol{\Sigma}_{k-1}\boldsymbol{\Sigma}_k^{-1} + \frac{1}{k}\left(\log_{\mu_k}(x_k)\right)^T\left(\log_{\mu_k}(x_k)\right) \tag{24}$$

Using $\mathbf{R}_k = \mathbf{V}_k\boldsymbol{\Lambda}_k{\mathbf{V}_k}^T$ Eq. (24) we get,

$$\mathbf{V}_k\boldsymbol{\Lambda}_k{\mathbf{V}_k}^T = \hat{\mathbf{V}}_{k-1}\left[(1-\lambda)\boldsymbol{\Lambda}_{k-1} + \lambda\hat{\mathbf{V}}^T\left(\log_{\mu_k}(x_k)\right)\left(\log_{\mu_k}(x_k)\right)^T\hat{\mathbf{V}}_k\right]\hat{\mathbf{V}}_{k-1}^T \tag{25}$$

Eigenperturbation approaches address the increasing computational cost of estimating covariance using Eqs. (24) at each time step as the sample size increases. This entails updating the covariance matrix's eigenvalues and eigenvectors. The parameter λ represents the memory depth and typically falls within the range $0 \le \lambda \le 1$, with specific values chosen based on requirements. In this context, λ can be set as $\frac{1}{k}$. The Eigenvector update is provided as $\mathbf{V}_k = \mathbf{V}_{k-1}\left(I + \boldsymbol{\Delta}_V\right)$ and the update of eigenvalue is given as, $\boldsymbol{\Lambda}_k = \left(\boldsymbol{\Lambda}_{k-1} + \boldsymbol{\Delta}_{\Lambda}\right)$. The eigenspaces are subjected to small perturbations $\boldsymbol{\Delta}V$ and $\boldsymbol{\Delta}\Lambda$. These perturbations can be substituted into Eq. (19), which can then be rewritten as follows:

$$\begin{aligned}\mathbf{V}_k\boldsymbol{\Lambda}_k{\mathbf{V}_k}^T &= \mathbf{V}_{k-1}\left[\boldsymbol{\Lambda}_{k-1} + \boldsymbol{\Delta}_{\Lambda} + \boldsymbol{\Lambda}_{k-1}{\boldsymbol{\Delta}_V}^T\right.\\ &\left.+\boldsymbol{\Delta}_V\boldsymbol{\Lambda}_{k-1} + \boldsymbol{\Delta}_{\Lambda}{\boldsymbol{\Delta}_V}^T + \boldsymbol{\Delta}_V\boldsymbol{\Delta}_{\Lambda}\right]{\mathbf{V}_{k-1}}^T\end{aligned} \tag{26}$$

Through a comparison of Eqs. (25) and (26), it is clear that the first-order perturbation, eliminating terms of second order (that is, $\boldsymbol{\Delta}\Lambda\boldsymbol{\Delta}V^T$ and $\boldsymbol{\Delta}V\boldsymbol{\Delta}\Lambda$), can be written as follows:

$$\begin{aligned}&\boldsymbol{\Delta}_{\Lambda} + \boldsymbol{\Lambda}_{k-1}{\boldsymbol{\Delta}_V}^T + \boldsymbol{\Delta}_V\boldsymbol{\Lambda}_{k-1}\\ &= \hat{\mathbf{V}}^T\left((1-\lambda)\boldsymbol{\Sigma}_k^{-1}\Delta\mu_k\Delta\mu_k^T\boldsymbol{\Sigma}_k^{-1} + \lambda\left(\log_{\mu_k}(x_k)\right)\left(\log_{\mu_k}(x_k)\right)^T\right)\hat{\mathbf{V}}_k\end{aligned} \tag{27}$$

The eigenspaces undergo updates accordingly after evaluating the perturbation matrices using Eq. (27). However, owing to the real-timenature of the framework, there might be ambiguity in the permutation of the updated eigenspaces. This ambiguity can be resolved by rearranging the eigenvectors based on the decreasing order of their corresponding eigenvalues. As alterations unfold in the system evolving within the manifold, the principal geodesics within the manifold are also defined. The framework projects the principal components back from $T_{\mu_k}M^p$ to M^p.

$$\psi_k = \mathrm{Exp}_{\mu_k}\left(\hat{\mathbf{V}}_k^T\left(\log_{\mu_k}(x_k)\right)\right) \tag{28}$$

Relying solely on monitoring changes in the eigenspace might not be sufficient to detect instances of damage. Therefore, employing a condition indicator capable of magnifying the impact of changes in the eigenspace becomes essential, thereby enhancing its detectability.

6. A note on the connection between RPCA on $\mathbb{R}^n$ and RPGA on S^2

The algorithm, RPGA, constitutes an approach to damage detection rooted in the domain of order eigenperturbation (FOEP). It finds its unique niche when dealing with data residing on the spherical manifold S^2. In this intricate mathematical framework, the data points are not just raw numerical values but are situated on the spherical surface, adding complexity to the analysis. To unravel the underlying structure, RPGA projects this data onto the tangent bundle, TS^2, a space where tangent vectors capture the local geometry of the manifold. The covariance matrix can be expressed as:

$$\mathbf{R}_k = \frac{k}{k-1}\mathbf{R}_{k-1} + \frac{1}{k-1}\left[\log_{\mu_k}(x_k)\right]\left[\log_{\mu_k}(x_k)\right]^T \tag{29}$$

the mean μ_k is obtained through the intrinsic formulation of the mean as expressed in Eq. (14). The principal geodesics are then extracted from this transformed space in real-time, effectively characterizing the essential features of the data. Operations on the tangent space become possible owing to the Euclidean-tangent space diffeomorphism. This process forms an eigenspace that encapsulates the intrinsic properties of the spherical data.

Now, the transformation of perspective makes this connection between RPGA and RPCA intriguing. Imagine merging the manifold S^2 and its associated tangent space TS^2 into a unified Euclidean subspace, which negates the projection of the data to TS^2. By doing so, we transition from the intricate spherical representation to a more conventional Euclidean space $\mathbb{R}^n$, and the block covariance matrix takes up the form

$$\mathbf{R}_k = \frac{k}{k-1}\mathbf{R}_{k-1} + \frac{1}{k-1}x_kx_k^T \tag{30}$$

In this new setting, the RPGA algorithm converges to RPCA, a widely used technique for data analysis in Euclidean spaces. This transition

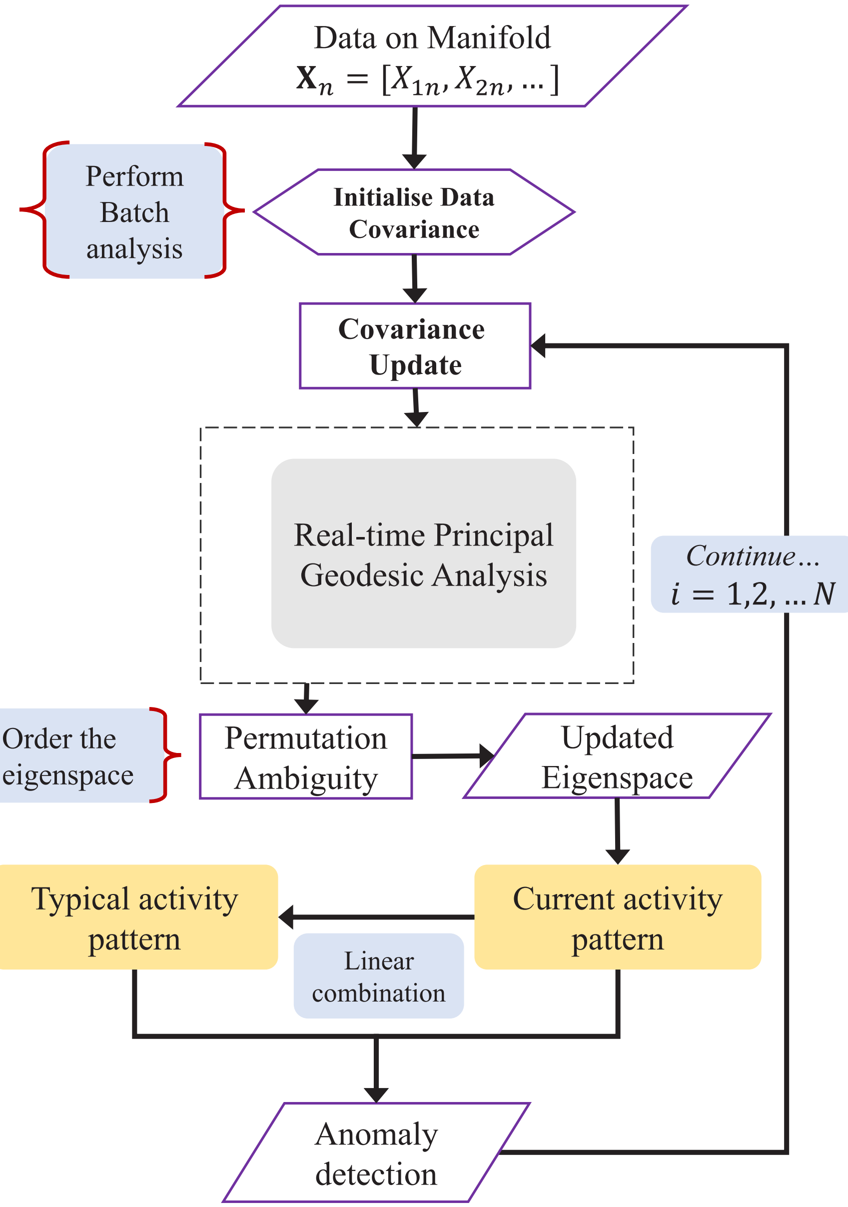

Fig. 3. A schematic of the proposed framework showcasing the functionality of the condition indicator.

highlights the interaction between different geometric spaces and how the choice of representation can significantly impact the selection and performance of data analysis algorithms, shedding light on the powerful connection between RPGA on S^2 and RPCA on $\mathbb{R}^n$.

6.1. Condition indicator (CI)

n this study, a novel approach has been developed to detect temporal damage in the evolving system manifold by introducing a new condition indicator. The CI calculates the dissimilarity between the current transformed vector and a reference pattern derived from a linear combination of the current pattern [29]. To ensure self-reliance on the algorithms, condition indicators (CI) are employed to evaluate changes in the updated eigenspace and accentuate these alterations. Changes in the system can be detected by comparing the current pattern with a base pattern. The current framework takes the response on the transformed space ψ_k as input for processing.

$$\mathcal{R}_k = \arg\max_{\mathbf{V}_k} \left(\psi_k \left(\psi_k \right)^T \right) \tag{31}$$

The current pattern is shaped by a sequence of Φ_k with a dimension of embedding d, and it is subsequently organized into a Hankel matrix.

$$\Gamma_k = \left[\mathcal{R}_k \quad \mathcal{R}_{k-1} \quad \mathcal{R}_{k-2} \quad \ldots \quad \mathcal{R}_{k-d+1} \right]^T \tag{32}$$

A reference pattern of the eigenstructure is created by linearly combining the current pattern components.

$$\rho_k = \eta \sum_{i=1}^{d} c_i \mathcal{R}_{k-i+1} \tag{33}$$

The extremum principle must be applied to optimize the linear combination coefficients c_i to estimate the reference pattern ρ_k. $\eta = 1/\sqrt{v}$ is used to compute this constant, where v represents the eigenvalues of the Hankel covariance matrix $\Gamma_k \Gamma_k^T$. A normalization constant, η, ensures that ρ_k forms an orthogonal vector. This procedure guarantees that the eigenstructure's properties are faithfully represented in the reference pattern.

$$c_k = \arg\max_{\gamma} \left\| \sum_{i=1}^{d} \gamma_k(i) \mathcal{R}_{t-i+1} \right\|^2 \tag{34}$$

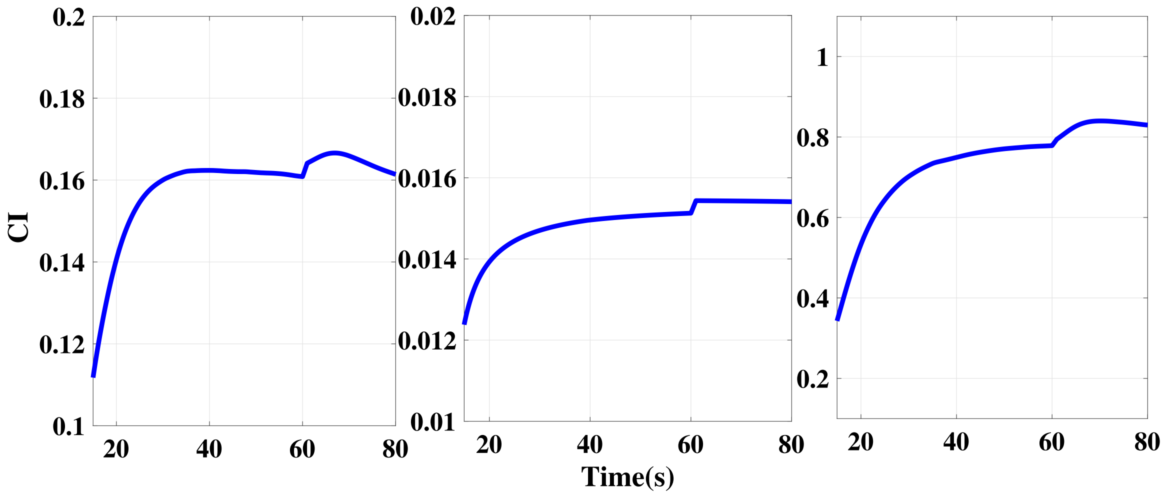

Fig. 4. Stochastic linear system: Representation of the condition indicator using RPCA framework.

The eigenvectors of the Hankel covariance matrix $\Gamma_k \Gamma_k^T$ are denoted by γ. Subsequently, the CI, which signifies the disparity between the current and reference patterns, is evaluated. This step is crucial for detecting any deviations or changes between the two patterns, aiding in identifying potential damage instances.

$$\mathbf{CI}(k) = \rho_{k-1}{}^T \mathcal{R}_k \tag{35}$$

This method detects differences between the reference and current patterns, thus pinpointing potential instances of damage. Any deviation in the values of the CI indicates damage occurring at that specific moment. Additionally, a flowchart depicting the functionality of the condition indicator within the RPGA framework is provided in Fig. 3.

7. Numerical experiments

This section presents the efficacy of the proposed RPGA framework for anomaly detection to three distinct systems: a stochastic geometric oscillator on S^2, and an inverted spherical pendulum suspended from a cart. This comprehensive exploration demonstrates RPGA's versatility and adaptability, making it a valuable tool for diverse real-world systems with complex dynamics.

7.1. Geometric description of a stochastic linear oscillator on S^2

Oscillators have garnered significant attention due to their capacity to simulate intricate physical phenomena and contemporary structures within Euclidean space. Presently, researchers are exploring the application of these oscillators in modeling satellite and drone trajectories, as well as controlling artificial limbs and modeling robots, within manifold spaces [30–32]. This section aims to furnish a geometrically precise solution of a linear oscillator situated on a sphere, thereby validating the effectiveness of the proposed algorithm. Towards this, consider

$$m\ddot{x} + c\mathbf{Q}\dot{x} + k\mathbf{Q}x = \sigma\dot{W} \tag{36}$$

where, m, c and k represents the generic system properties, and, $\mathbf{Q} = \begin{bmatrix} 2 & -1 & 0 \\ -1 & 2 & -1 \\ 0 & -1 & 1 \end{bmatrix}$. σ is a representation of the magnitude of the stochastic excitation $\dot{W}$. Eq. (36) characterizes a single-mass three-degree-of-freedom (3DOF) system, with its degrees of freedom designated along the x, y, and z directions, denoted as $(x_1, x_2, x_3) \in \mathbb{R}^3$. In the state-space representation, Eq. (36) can be represented as,

$$\begin{aligned} \dot{x} &= y \\ \dot{y} &= -\tfrac{c}{m}\mathbf{Q}y - \tfrac{k}{m}\mathbf{Q}x + \sigma\dot{W} \end{aligned} \tag{37}$$

Operating within the Euclidean space and devoid of geometric constraints, the RPCA algorithm [8], tailored for Euclidean spaces, effectively discerns instances of damage in the system. However, the complexity intensifies when the system is confined to evolve on a spherical surface, introducing constraints. In this scenario, the task of damage identification becomes more intricate. The foundational work outlined in literature [19] provides the base for extending the conventional potential function to operate on the curved space by substituting the generic distance on the Euclidean space with the Riemannian distance. In the current study, $\mathfrak{d}(a,b) = |\log_a(b)|_a$ is the Riemannian distance function. In the context of the geometric oscillator under consideration, driven by a white Gaussian process $\dot{\mathrm{W}}$, the expressions for kinetic and potential energies are delineated as follows:

$$K = \frac{1}{2}\langle\omega,\omega\rangle, \quad V = \frac{1}{2}\gamma\mathfrak{d}^2(p,r) \tag{38}$$

Through the formulation of the Lagrangian function and the application of the stochastic variational principle, one can derive the governing equation for the motion of the undertaken system:

$$\dot{\omega} = \gamma\left(p \times \log_p(r)\right) - \eta\langle\omega,\omega\rangle^{(\nu-1)}(\omega \times p) + Fcos(\zeta t) + \beta\dot{\mathrm{W}} \tag{39}$$

In this context, $(p,\omega) \in \mathrm{S}^2 \times \mathrm{T}_p\mathrm{S}^2$ represent the state variables. The damping coefficient is denoted as $\eta = 0.5 \in \mathbb{R}$, the damping degree as $\nu = 1.3 \in \mathbb{R}$, the coefficient $\gamma = 1 \in \mathbb{R}$, and $r = [1,0,0] \in \mathrm{S}^2$ signifies the pivotal point. The kinematic equations are given by $\dot{p} = \omega \times p$. The harmonic excitation has an amplitude $F = 0.1$ and a forcing frequency $\zeta = 1$. Simulation on S^2 with the canonical metric utilizes results from [19] to estimate distance metric and matrix logarithm. Initial position and angular velocity are $[\sqrt{3}; \sqrt{3}; \sqrt{3}]^T$ and $[0.2; 0.3; -0.4]^T$, respectively. The system exhibits an anomaly that is artificially introduced by abruptly reducing the coefficient γ to 80% of the existing stiffness at 6000th sample. The obtained results for the damage identification are illustrated in Fig. 5, wherein a distinct and prominent peak at the 6000th sample clearly indicates the presence of the anomaly within the system. Whereas, Fig. 4 shows the anomaly identification using Euclidean based algorithm RPCA, which provides an erroneous eigenspace thereby fails to provide the instance of anomaly in the undertaken system.

7.2. Inverted pendulum cart system moving on a rough surface

This section provides the efficacy of the proposed algorithm for the anomaly detection of the inverted spherical pendulum cart system

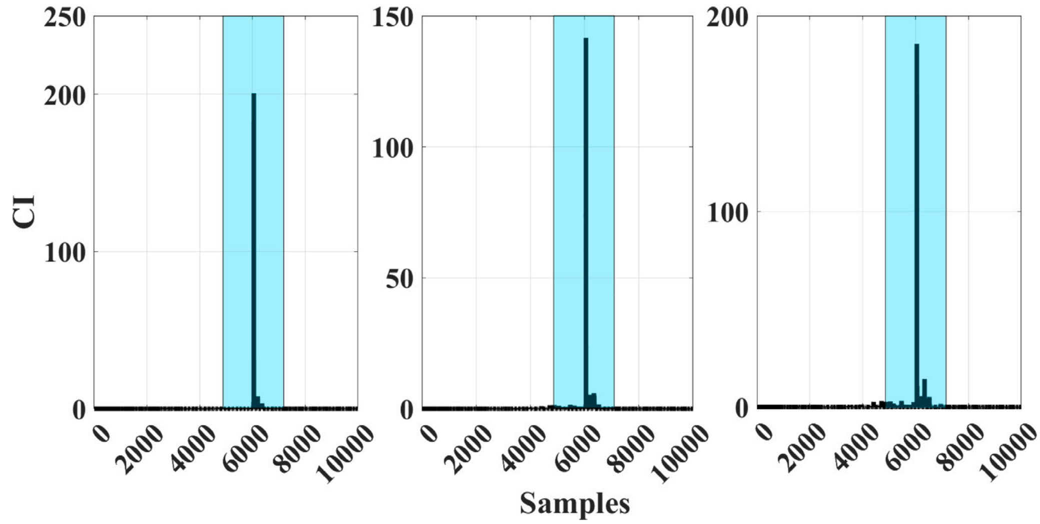

Fig. 5. Geometric stochastic linear system: Representation of the condition indicator using manifold based RPGA framework.

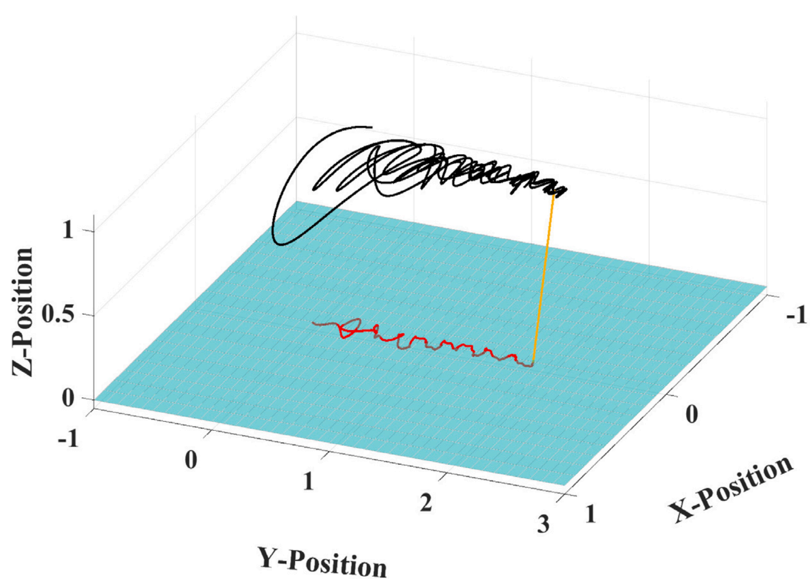

Fig. 6. Stochastic pendulum cart system: Global trajectory of the cart in $\mathbb{R}^3$ (red line) and pendulum on S^2 (black line) with the initial conditions $x(0) = [0,0,0], \dot{x} = [0,0,0], q = [0,0,-1], \omega = [0.2,0.3,0.5]$. (For interpretation of the references to color in this figure legend, the reader is referred to the web version of this article.)

traversing on a rough surface with $p \in S^2$ and $\omega \in T_x S^2$ are the position and angular velocity of the pendulum, and, $x \in \mathbb{R}^3$ and $\dot{x} \in \mathbb{R}^3$ being displacement and velocity of the cart. The Lagrangian of the system can be formulated as:

$$\hat{L}(p, x_c, \omega, \dot{x_c}) = \frac{1}{2}(M_c + m)\langle \dot{x_c}, \dot{x_c}\rangle - ml\dot{x_c}^T p^\Lambda \omega + \frac{1}{2}ml^2\langle \omega, \omega\rangle - mgle_3^T p - \frac{1}{2}k\langle x_c, x_c\rangle \tag{40}$$

where $e_3 = [0,0,1]$ will be in the positive z direction. The equation of motion is directly formulated in the Lie algebra $(\hat{\mathbf{p}}, \hat{\boldsymbol{\omega}}) \in T_\xi S^2$ in the state space form after the kinematic equation of the pendulum integrating the stochastic term is included:

$$\mathrm{d}\underbrace{\begin{bmatrix}\hat{\mathbf{p}}\\ \hat{\boldsymbol{\omega}}\\ x_c\\ \dot{x}_c\end{bmatrix}}_{\tau} = \underbrace{\begin{bmatrix}\omega^\Lambda\\ -\left(A_{11}\left(mglp\times r\right) + A_{12}\left(ml\left(\omega^\Lambda\right)^2 p + C\dot{x_c} + Kx_c\right)\right)^\Lambda\\ \dot{x}_c\\ -A_{21}\left(mglp\times r\right) - A_{22}\left(ml\left(\omega^\Lambda\right)^2 p + C\dot{x_c} + Kx_c\right)\end{bmatrix}}_{\gamma}\mathrm{d}t$$

$$+\underbrace{\begin{bmatrix}0\\ \left(A_{11}p\times\beta_1\right)\mathrm{d}B_1 + \left(A_{12}\beta_2\right)\mathrm{d}B_2\\ 0\\ \left(A_{21}p\times\beta_1\right)\mathrm{d}B_1 + \left(A_{22}\beta_2\right)\mathrm{d}B_2 + \sigma\mathrm{d}B_3\end{bmatrix}}_{\delta_r\ \mathrm{dB}_r} \tag{41}$$

where, $\begin{bmatrix}(A_{11})_{3\times3} & (A_{12})_{3\times2}\\ (A_{21})_{2\times3} & (A_{22})_{2\times2}\end{bmatrix} = \begin{bmatrix}ml^2 I_3 & mlp^\Lambda\\ -mlp^\Lambda & (M+m)\end{bmatrix}^{-1}$. For this study's simulation, the parameters used are $M_c = 100$ kg, $m = 0.9$ kg, $l = 1$ m, $k = 1000$ N/m, and $g = 9.81$ m/s^2. Here, $\hat{p}_0 = [0,0,-1]^T$ and $\hat{\omega}_0 = [0.2,0.3,0.5]^T$. The stochastic differential equation (SDE) detailed in Eq. (41), governing $\hat{\mathbf{p}}$ and $\hat{\boldsymbol{\omega}}$, conforms to the Lie algebraic structure and undergoes simulation using the geometric Ito-Taylor–1.5 framework. Regarding the SDEs in Eq. (41), we obtain the Kolmogorov operators for variables x_c and $\dot{x}_c$, and then apply the proposed framework for updating the system states. The surface roughness is simulated using a stochastic process in z-direction with zero mean and σ as 0.1. The inverted Pendulum-cart system exhibits an anomaly that is artificially introduced by abruptly reducing the stiffness of the cart to 80% of the

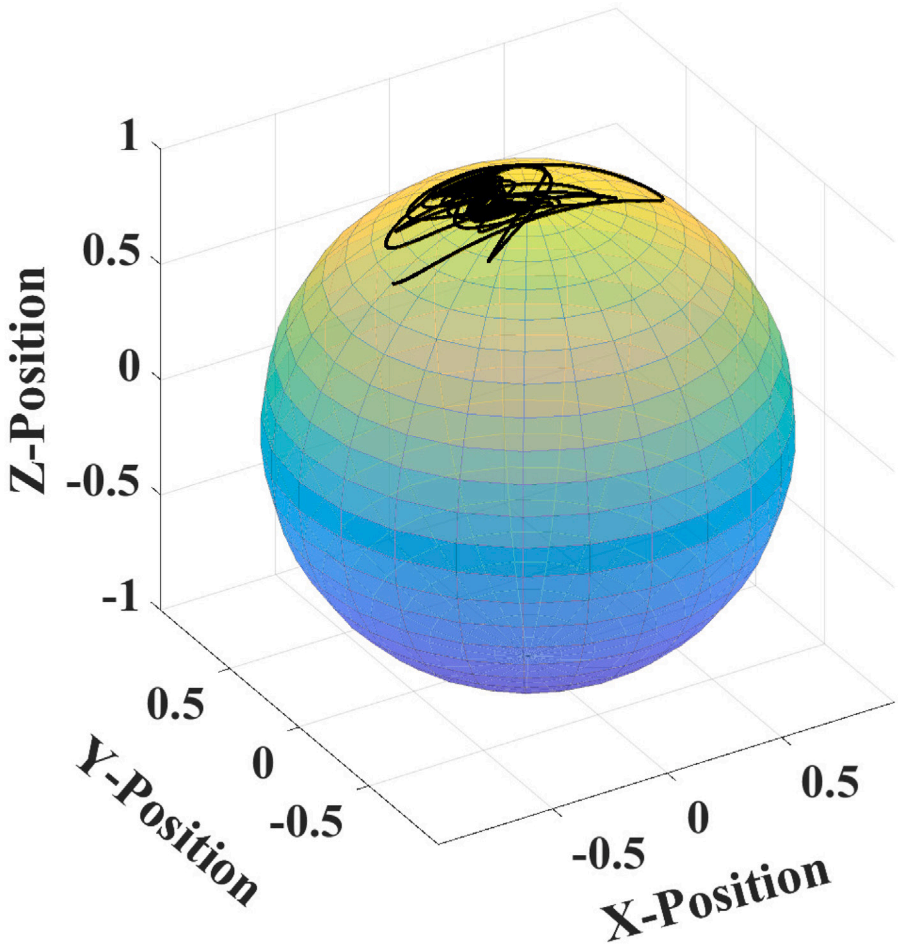

Fig. 7. Stochastic pendulum cart system: Local trajectory of the pendulum on S^2 with the initial conditions $q = [0, 0, -1], \omega = [0.2, 0.3, 0.5]$.

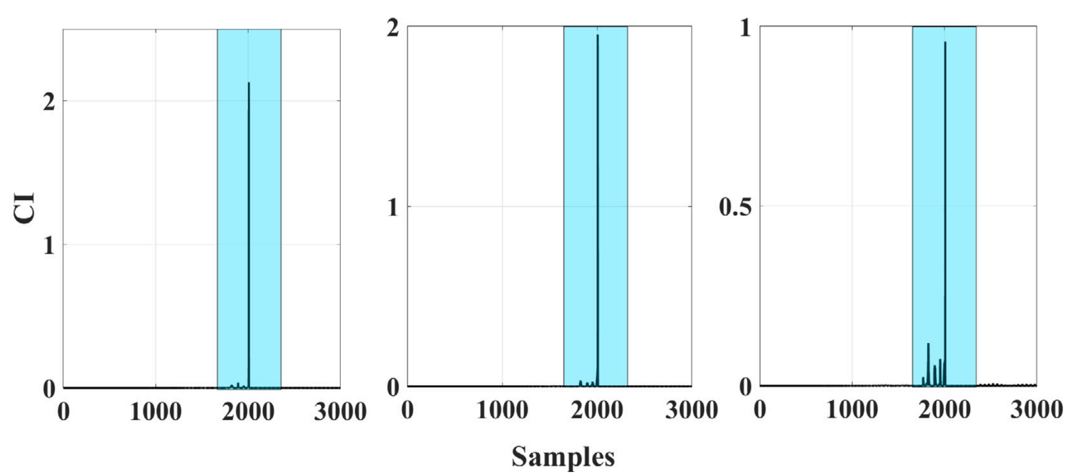

Fig. 8. Stochastic pendulum cart system: Representation of the condition indicator using manifold based RPGA framework.

original stiffness at the 2000th sample. Fig. 6 shows the trajectory of the cart (red line) on $\mathbb{R}^3$ and the trajectory of the inverted spherical pendulum (black line) on S^2. For the better clarification Fig. 7 shows that the response of inverted pendulum lies on a unit 2-sphere. The obtained results for the damage identification are illustrated in Fig. 8, wherein a distinct and prominent peak at the 2000th sample clearly indicates the presence of the anomaly within the system. For the comparison of the effectiveness of the proposed algorithm with the offline algorithm PGA, Fig. 9 presents the condition indicator for the undertaken system through the use of offline PGA algorithm. A change in mean of CI can be observed at around 2000 samples in Fig. 9, which shows that PGA algorithm can estimate the approximate time of the damage. This limitation arises owing to the offline nature of the algorithm. From Figs. 8 and 9 it is clear that the proposed framework accurately identifies the precise time-point of the anomaly in the system. In regard to sensitivity analysis, Fig. 10 illustrates the confidence intervals (CIs) for the system under various damage scenarios. The figure reveals that the proposed framework can effectively detect damage instances of up

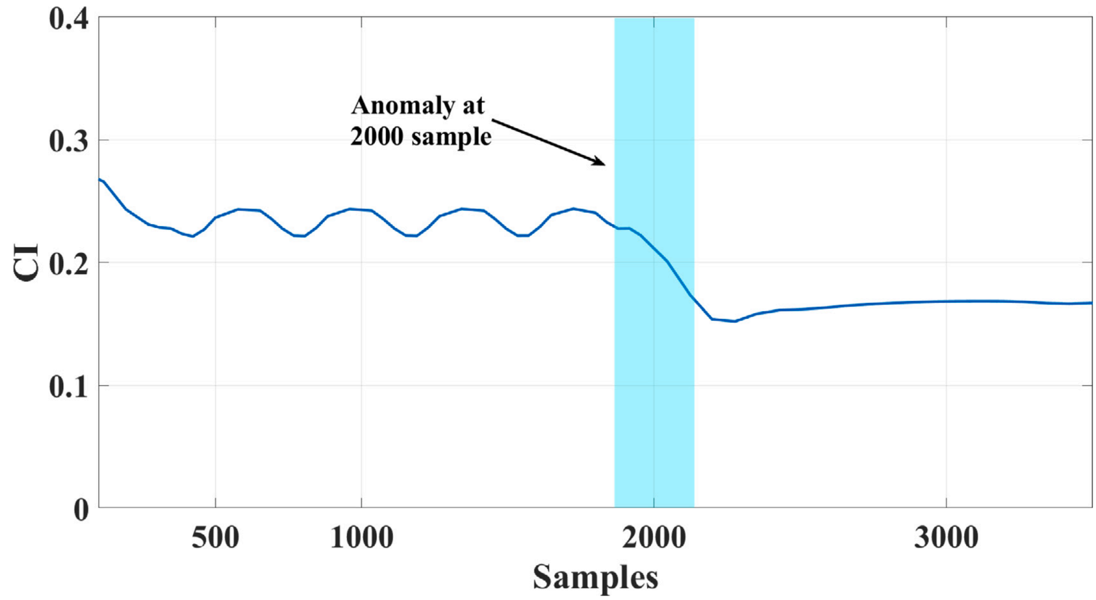

Fig. 9. Stochastic pendulum cart system: Representation of the condition indicator using manifold based PGA framework.

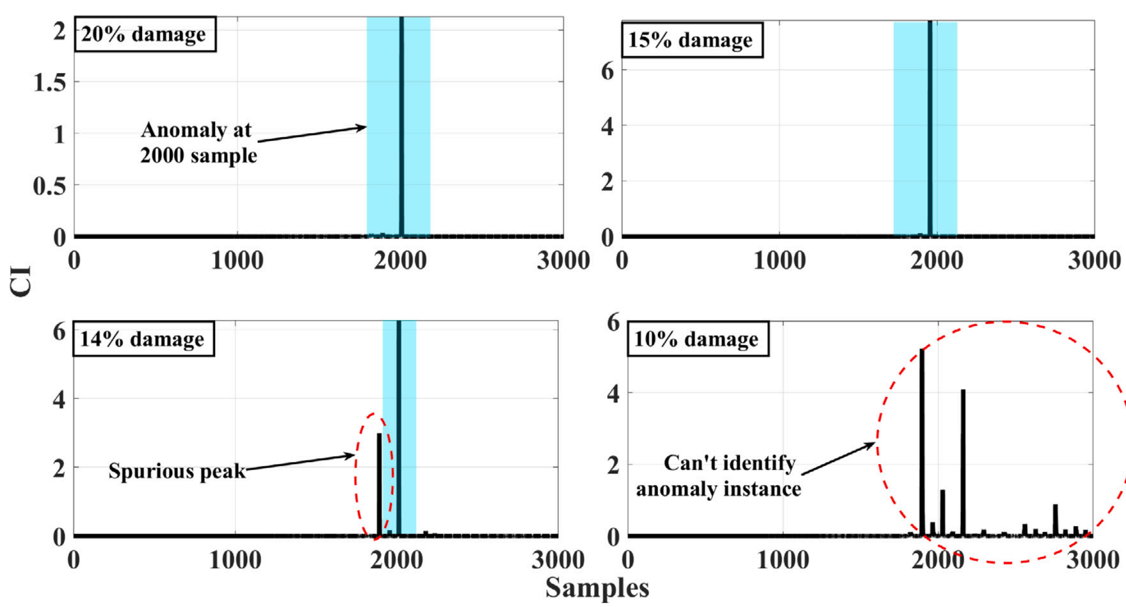

Fig. 10. Stochastic pendulum cart system: Damage sensitivity test for 20%, 15%, 14% and 10% damage.

to 15%, but beyond that threshold, it exhibits spurious peaks alongside the damage indication. Notably, the proposed algorithm fails to identify any damage at or below the 10% threshold for structural damage which is the same conclusion as in the case of spherical pendulum system. Another aspect of the analysis involves conducting a study to assess the sensitivity of parameters within the system under consideration. This examination delves into how variations or perturbations in specific parameters affect the overall behavior and performance of the system. By systematically varying the parameters M_c, m, l and k independently, while maintaining the remaining parameters constant, insights can be gleaned into the system's response and its susceptibility to changes in different factors. The damage detectability for varying parameter scenarios is given in Table 1. This parameter sensitivity study provides valuable information for understanding the system's robustness, identifying critical parameters that significantly influence its behavior, and refining the modeling and control strategies to enhance overall performance.

8. Conclusions

This research introduces Real-time Principal Geodesic Analysis (RPGA) as a novel method for conducting condition monitoring of systems operating within differentiable manifolds. RPGA offers a robust framework for extracting meaningful information from manifold-based data, enabling more accurate and precise health assessments. furthermore, the study systematically applies RPGA to distinct systems: the stochastic geometric oscillator on S^2, and a spherical pendulum suspended from a cart. This comprehensive exploration demonstrates RPGA's versatility and adaptability, making it a valuable tool for diverse real-world systems with complex dynamics. To gauge RPGA's effectiveness, the research performs a comparative analysis by contrasting condition monitoring results obtained through RPGA with those generated by RPCA, a monitoring scheme tailored for $\mathbb{R}^2$. This rigorous comparison underscores RPGA's superiority in providing accurate health assessments for systems on differentiable manifolds, thereby

Table 1
Damage detectability for varying parameters for inverted pendulum cart system.

M_c	Detectability	m	Detectability	l	Detectability	k	Detectability
10	Yes	0.01	Yes	0.1	Yes	100	Yes
50	Yes	0.5	Yes	0.5	Yes	500	Yes
200	Yes	5	No	1.5	Yes	2000	Yes
400	No	10	No	2.0	No	3500	Yes
600	No	20	No	2.5	No	5000	Yes

emphasizing its practical significance in the field of complex systems analysis. Moreover, the study includes a sensitivity test to determine the threshold at which the proposed RPGA algorithm starts producing erroneous results. Findings reveal that the proposed framework effectively detects damage instances of up to 15%, but beyond this threshold, it exhibits spurious peaks alongside damage indications. Notably, RPGA fails to identify any damage at or below the 10% threshold for structural damage.

To address the limitation of detecting damage below 10%, future research could explore enhancements such as incorporating higher-order perturbation terms or incorporating the error arising owing to the consideration of first order error perturbation. Other possibilities include leveraging machine learning algorithms to improve sensitivity and accuracy. These potential improvements could significantly extend the applicability and effectiveness of RPGA in various engineering contexts, ensuring more reliable condition monitoring and damage detection in complex systems.

CRediT authorship contribution statement

Satyam Panda: Writing – original draft, Visualization, Validation, Software, Methodology, Investigation, Formal analysis, Data curation. **Breiffni Fitzgerald:** Writing – review & editing, Supervision. **Budhaditya Hazra:** Writing – review & editing, Visualization, Supervision, Resources, Conceptualization.

Declaration of competing interest

The authors declare that they have no known competing financial interests or personal relationships that could have appeared to influence the work reported in this paper.

Data availability

No data was used for the research described in the article.

Acknowledgment

Satyam Panda and Breiffni Fitzgerald would like to acknowledge the support provided by the Science Foundation Ireland under the NexSys project (21/SPP/3756).

References

[1] S. Sommer, F. Lauze, M. Nielsen, Optimization over geodesics for exact principal geodesic analysis, Adv. Comput. Math. 40 (2014) 283–313.
[2] P.T. Fletcher, C. Lu, S.M. Pizer, S. Joshi, Principal geodesic analysis for the study of nonlinear statistics of shape, IEEE Trans. Med. Imaging 23 (8) (2004) 995–1005.
[3] C.G. Gebhardt, M.C. Steinbach, R. Rolfes, Understanding the nonlinear dynamics of beam structures: a principal geodesic analysis approach, Thin-Walled Struct. 140 (2019) 357–372.
[4] S. Sommer, F. Lauze, S. Hauberg, M. Nielsen, Manifold valued statistics, exact principal geodesic analysis and the effect of linear approximations, in: Computer Vision–ECCV 2010: 11th European Conference on Computer Vision, Heraklion, Crete, Greece, September 5-11, 2010, Proceedings, Part VI 11, Springer, 2010, pp. 43–56.
[5] W. Li, H.H. Yue, S. Valle-Cervantes, S.J. Qin, Recursive PCA for adaptive process monitoring, J. Process Control 10 (5) (2000) 471–486.
[6] M.A. DE Oliveira, D.J. Inman, PCA-based method for damage detection exploring electromechanical impedance in a composite beam, Struct. Health Monit. 2015 (2015).
[7] M. Mirmomeni, C. Lucas, B. Araabi, B. Moshiri, M. Bidar, Recursive spectral analysis of natural time series based on eigenvector matrix perturbation for online applications, IET Signal Process. 5 (6) (2011) 515–526.
[8] B. Bhowmik, T. Tripura, B. Hazra, V. Pakrashi, First-order eigen-perturbation techniques for real-time damage detection of vibrating systems: Theory and applications, Appl. Mech. Rev. 71 (6) (2019).
[9] S. Panda, T. Tripura, B. Hazra, First-order error-adapted eigen perturbation for real-time modal identification of vibrating structures, J. Vib. Acoust. 143 (5) (2021) 051001.
[10] B. Bhowmik, S. Panda, B. Hazra, V. Pakrashi, Feedback-driven error-corrected single-sensor analytics for real-time condition monitoring, Int. J. Mech. Sci. 214 (2022) 106898.
[11] M. Misra, H.H. Yue, S.J. Qin, C. Ling, Multivariate process monitoring and fault diagnosis by multi-scale PCA, Comput. Chem. Eng. 26 (9) (2002) 1281–1293.
[12] Y. Wang, X. Ma, P. Qian, Wind turbine fault detection and identification through PCA-based optimal variable selection, IEEE Trans. Sustain. Energy 9 (4) (2018) 1627–1635.
[13] M. Rezamand, M. Kordestani, R. Carriveau, D.S.-K. Ting, M. Saif, A new hybrid fault detection method for wind turbine blades using recursive PCA and wavelet-based PDF, IEEE Sens. J. 20 (4) (2019) 2023–2033.
[14] P. Cahill, B. Hazra, R. Karoumi, A. Mathewson, V. Pakrashi, Vibration energy harvesting based monitoring of an operational bridge undergoing forced vibration and train passage, Mech. Syst. Signal Process. 106 (2018) 265–283.
[15] S. Panda, T. Tripura, B. Hazra, Online damage detection of earthquake-excited structure based on near real-time envelope extraction, Struct. Health Monit. 21 (2) (2022) 298–319.
[16] R. Rana, T. Soong, Parametric study and simplified design of tuned mass dampers, Eng. Struct. 20 (3) (1998) 193–204.
[17] M.S. Allen, M.W. Sracic, S. Chauhan, M.H. Hansen, Output-only modal analysis of linear time-periodic systems with application to wind turbine simulation data, Mech. Syst. Signal Process. 25 (4) (2011) 1174–1191.
[18] T. Lee, M. Leok, N.H. McClamroch, Global Formulations of Lagrangian and Hamiltonian Dynamics on Manifolds, Springer, 2017.
[19] S. Fiori, I. Cervigni, M. Ippoliti, C. Menotta, Synthetic nonlinear second-order oscillators on Riemannian manifolds and their numerical simulation, Discrete Contin. Dyn. Syst. Ser. B 27 (3) (2022) 1227.
[20] Q. Pan, T. Rabczuk, C. Chen, G. Xu, K. Pan, Isogeometric analysis of minimal surfaces on the basis of extended Catmull–Clark subdivision, Comput. Methods Appl. Mech. Engrg. 337 (2018) 128–149.
[21] G. Xu, T. Rabczuk, E. Güler, Q. Wu, K.-c. Hui, G. Wang, Quasi-harmonic Bézier approximation of minimal surfaces for finding forms of structural membranes, Comput. Struct. 161 (2015) 55–63.
[22] D. Lazar, L. Lin, Scale and curvature effects in principal geodesic analysis, J. Multivariate Anal. 153 (2017) 64–82.
[23] H. Salehian, G. Cheng, B.C. Vemuri, J. Ho, Recursive estimation of the stein center of SPD matrices and its applications, in: Proceedings of the IEEE International Conference on Computer Vision, 2013, pp. 1793–1800.
[24] A. Roffel, R. Lourenco, S. Narasimhan, S. Yarusevych, Adaptive compensation for detuning in pendulum tuned mass dampers, J. Struct. Eng. 137 (2) (2011) 242–251.
[25] D.M. Lazar, Scale and Dimension Reduction in Symmetric Spaces (Ph.D. thesis), Central Michigan University, 2015.
[26] A.N. Pressley, Elementary Differential Geometry, Springer Science & Business Media, 2010.
[27] S. Fiori, Nonlinear damped oscillators on Riemannian manifolds: Fundamentals, J. Syst. Sci. Complex. 29 (2016) 22–40.
[28] H. Karcher, Riemannian center of mass and mollifier smoothing, Commun. Pure Appl. Math. 30 (5) (1977) 509–541.
[29] T. Idé, H. Kashima, Eigenspace-based anomaly detection in computer systems, in: Proceedings of the Tenth ACM SIGKDD International Conference on Knowledge Discovery and Data Mining, 2004, pp. 440–449.
[30] E. Celledoni, E. Çokaj, A. Leone, D. Murari, B. Owren, Lie group integrators for mechanical systems, Int. J. Comput. Math. 99 (1) (2022) 58–88.
[31] R.J. Burston, Earth-like planetary magnetotails as non-linear oscillators, Ann. Geophys. Discuss. (2020) 1–32.
[32] S. Aoi, K. Tsuchiya, Locomotion control of a biped robot using nonlinear oscillators, Auton. Robots 19 (3) (2005) 219–232.